Cross-Section Analysis in Python

Robbie van Leeuwen[a]

[a]*Delft University of Technology, Faculty of Civil Engineering and Geosciences, P.O. Box 5048, 2600GA Delft, The Netherlands*

Abstract

A python program was created to analyse an arbitrary cross-section using the finite element method and output properties to be used in structural design. The program also calculates normal and shear stresses resulting from axial force, bending moments, torsion moment and transverse shear forces. This paper summarises the methodology and theory behind the computation of the various properties.

Keywords: finite element method, cross-section analysis, python

1. Introduction

The analysis of homogenous cross-sections is particularly relevant in structural design, in particular for the design of steel structures, where complex built-up sections are often utilised. Accurate warping independent properties, such as the second moment of area and section modulii, are crucial input for structural analysis and stress verification. Warping dependent properties, such as the Saint-Venant torsion constant and warping constant are essential in the verification of slender steel structures when lateral-torsional buckling is critical.

Warping independent properties for basic cross-sections are relatively simple to calculate by hand. However accurate warping independent properties, even for the most basic cross-section, require solving several boundary value partial differential equations. This necessitates numerical methods in the calculation of these properties, which can be extended to arbitrary complex sections.

This paper describes the theory and application of the finite element method to cross-sectional analysis. An arbitrary cross-section, as shown in Figure 1, is defined by a series of points, segments and holes, and a cross-sectional analysis and stress analysis is performed.

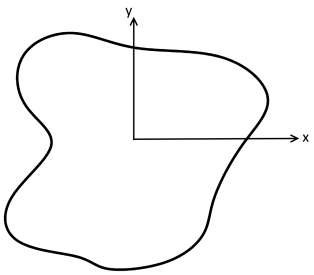

Figure 1: Arbitrary cross-section with adopted axis convention.

2. Mesh Generation

The cross-section is meshed into quadratic superparametric[1] triangular elements using the *meshpy* library for Python, which utilises the package, *Triangle*, which is a two dimensional quality mesh generator and delaunay triangulator written by Jonathan Shewchuk for C++. For the calculation of warping independent (area) properties, the mesh quality is not important as superparametric elements have a constant Jacobian. However, for the calculation of warping dependent properties, mesh quality and refinement is critical and thus the user is encouraged to ensure an adequate mesh is generated.

3. Finite Element Preliminaries

3.1. Element Type

Quadratic six-noded triangular elements were implemented in the program in order to utilise the finite element formulations for calculating the section properties. Figure 2 shows a typical six-noded triangular element.

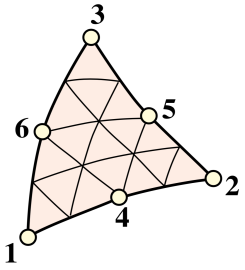

Figure 2: Six noded triangular element [1].

The quadratic triangular element was used due to the ease of mesh generation and convergence advantages over the linear triangular element.

Email address: robbie.vanleeuwen@gmail.com (Robbie van Leeuwen)

[1]The edges of the quadratic superparametric triangle are straight and they have their mid-nodes located at the mid-point between adjacent corner nodes

3.2. Isoparametric Representation

An isoparametric coordinate system has been used to evaluate the shape functions of the parent element and map them to a generalised triangular element within the mesh. Three independent isoparametric coordinates (η, ξ, ζ) are used to map the six-noded triangular element as shown in Figure 3.

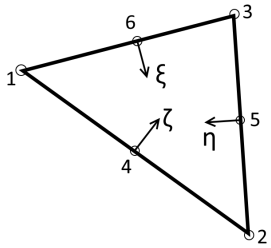

Figure 3: Isoparametric coordinates for the two dimensional triangular element.

3.2.1. Shape Functions

The shape functions for the six-noded triangular element in terms of the isoparametric coordinates are as follows:

$$\begin{aligned} N_1 &= \eta(2\eta - 1) \\ N_2 &= \xi(2\xi - 1) \\ N_3 &= \zeta(2\zeta - 1) \\ N_4 &= 4\eta\xi \\ N_5 &= 4\xi\zeta \\ N_6 &= 4\eta\zeta \end{aligned} \tag{1}$$

The above shape functions can be combined into the shape function row vector: $\mathbf{N} = [N_1\, N_2\, N_3\, N_4\, N_5\, N_6]$.

3.2.2. Cartesian Partial Derivatives

The partial derivatives of the shape functions with respect to the cartesian coordinates, denoted as the **B** matrix, are required in the finite element formulations of various section properties. Felippa [1] describes the multiplication of the *Jacobian matrix* (**J**) and the partial derivative matrix (**P**):

$$\mathbf{J}\,\mathbf{P} = \begin{bmatrix} 1 & 1 & 1 \\ \sum x_i \frac{\partial N_i}{\partial \eta} & \sum x_i \frac{\partial N_i}{\partial \xi} & \sum x_i \frac{\partial N_i}{\partial \zeta} \\ \sum y_i \frac{\partial N_i}{\partial \eta} & \sum y_i \frac{\partial N_i}{\partial \xi} & \sum y_i \frac{\partial N_i}{\partial \zeta} \end{bmatrix} \begin{bmatrix} \frac{\partial \eta}{\partial x} & \frac{\partial \eta}{\partial y} \\ \frac{\partial \xi}{\partial x} & \frac{\partial \xi}{\partial y} \\ \frac{\partial \zeta}{\partial x} & \frac{\partial \zeta}{\partial y} \end{bmatrix} = \begin{bmatrix} 0 & 0 \\ 1 & 0 \\ 0 & 1 \end{bmatrix} \tag{2}$$

The determinant of the *Jacobian matrix* scaled by one half is equal to the Jacobian:

$$J = \frac{1}{2} \det \mathbf{J} \tag{3}$$

Equation 2 can be re-arranged to evaluate the partial derivate matrix (**P**):

$$\mathbf{P} = \mathbf{J}^{-1} \begin{bmatrix} 0 & 0 \\ 1 & 0 \\ 0 & 1 \end{bmatrix} \tag{4}$$

As described in [1], the derivates of the shape functions can be evaluated using the above expressions:

$$\underset{[6\text{ x }2]}{\mathbf{B}^{\mathrm{T}}} = \underset{[6\text{ x }2]}{\begin{bmatrix} \frac{\partial N_i}{\partial x} & \frac{\partial N_i}{\partial y} \end{bmatrix}} = \underset{[6\text{ x }3]}{\begin{bmatrix} \frac{\partial N_i}{\partial \eta} & \frac{\partial N_i}{\partial \xi} & \frac{\partial N_i}{\partial \zeta} \end{bmatrix}} \underset{[3\text{ x }2]}{\begin{bmatrix} \mathbf{P} \end{bmatrix}} \tag{5}$$

where the derivatives of the shape functions with respect to the isoparametric parameters can easily be evaluated from Equation 1, resulting in the following expression for the **B** matrix:

$$\mathbf{B}^{\mathrm{T}} = \begin{bmatrix} 4\eta - 1 & 0 & 0 \\ 0 & 4\xi - 1 & 0 \\ 0 & 0 & 4\zeta - 1 \\ 4\xi & 4\eta & 0 \\ 0 & 4\zeta & 4\xi \\ 4\zeta & 0 & 4\eta \end{bmatrix} \mathbf{J}^{-1} \begin{bmatrix} 0 & 0 \\ 1 & 0 \\ 0 & 1 \end{bmatrix} \tag{6}$$

3.3. Numerical Integration

Three different integration schemes are utilised in the cross-section analysis in order to evaluate the integrals of varying order polynomials. The one point, three point and six point integration schemes are summarised in Figure 4. The locations and weights of the Gauss points are summarised in Table 1.

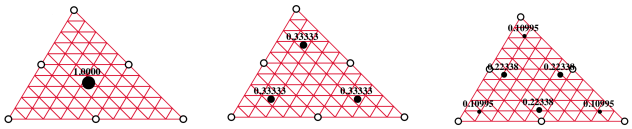

(a) 1 pt. integration; p-degree = 1.
(b) 3 pt. integration; p-degree = 2.
(c) 6 pt. integration; p-degree = 4.

Figure 4: Six-noded triangle integration schemes with maximum degree of polynomial that is evaluated exactly [1].

Scheme	η-location	ξ-location	ζ-location	weight
1 pt.	$\frac{1}{3}$	$\frac{1}{3}$	$\frac{1}{3}$	1
3 pt.	$\frac{2}{3}$	$\frac{1}{6}$	$\frac{1}{6}$	$\frac{1}{3}$
	$\frac{1}{6}$	$\frac{2}{3}$	$\frac{1}{6}$	$\frac{1}{3}$
	$\frac{1}{6}$	$\frac{1}{6}$	$\frac{2}{3}$	$\frac{1}{3}$
6 pt.	$1 - 2g_2$	g_2	g_2	w_2
	g_2	$1 - 2g_2$	g_2	w_2
	g_2	g_2	$1 - 2g_2$	w_2
	g_1	g_1	$1 - 2g_1$	w_1
	$1 - 2g_1$	g_1	g_1	w_1
	g_1	$1 - 2g_1$	g_1	w_1

Table 1: Locations and weights for the numerical integration schemes [1].

The parameters for the six point numerical integration are shown in Equation 7.

$$
\begin{aligned}
g_{1,2} &= \frac{1}{18}\left(8 - \sqrt{10} \pm \sqrt{38 - 44\sqrt{\frac{2}{5}}}\right) \\
w_{1,2} &= \frac{620 \pm \sqrt{213125 - 53320\sqrt{10}}}{3720}
\end{aligned}
\tag{7}
$$

Bringing together the isoparametric representation of the six-noded triangular element and numerical integration, the integration of a function $f(\eta, \xi, \zeta)$ proves to be simpler than integrating the corresponding function $f(x, y)$ over the cartesian element [2]. The transformation formula for integrals is:

$$
\begin{aligned}
\int_\Omega f(x,y)\,dx\,dy &= \int_{\Omega_r} f(\eta,\xi,\zeta)\,J\,d\eta\,d\xi\,d\zeta \\
&= \sum_i^n w_i f(\eta_i,\xi_i,\zeta_i)\,J_i
\end{aligned}
\tag{8}
$$

where the sum is taken over the integration points, w_i is the weight of the current integration point and J_i is the Jacobian at the current integration point[2].

3.4. Extrapolation to Nodes

The most optimal location to sample stresses are at the integration points, however the results are generally plotted using nodal values. As a result, the stresses at the integration points need to be extrapolated to the nodes of the element. The extrapolated stresses at the nodes ($\tilde{\boldsymbol{\sigma}}_g$) can be calculated through the multiplication of a smoothing matrix ($\mathbf{H}$) and the stresses at the integration points ($\boldsymbol{\sigma}_g$) [2]:

$$
\tilde{\boldsymbol{\sigma}}_g = \mathbf{H}^{-1}\,\boldsymbol{\sigma}_g \tag{9}
$$

where the $\mathbf{H}$ matrix contains the row vectors of the shape functions at each integration point:

$$
\mathbf{H} = \begin{bmatrix}
\mathbf{N}(\eta_1,\xi_1,\zeta_1) \\
\mathbf{N}(\eta_2,\xi_2,\zeta_2) \\
\mathbf{N}(\eta_3,\xi_3,\zeta_3) \\
\mathbf{N}(\eta_4,\xi_4,\zeta_4) \\
\mathbf{N}(\eta_5,\xi_5,\zeta_5) \\
\mathbf{N}(\eta_6,\xi_6,\zeta_6)
\end{bmatrix}
\tag{10}
$$

Where two or more elements share the same node, nodal averaging is used to evaluate the nodal stress.

3.5. Lagrangian Multiplier

As described in Sections 4.9 and 4.10, partial differential equations are to be solved with purely Neumann boundary conditions. In the context of the torsion and shear problem, this involves the inversion of a nearly singular global stiffness matrix. After shifting the domain such that the centroid coincides with the global origin, the Lagrangian multiplier method is used to solve the set of linear equations of the form $\mathbf{Ku} = \mathbf{F}$ by introducing an extra constraint on the solution vector whereby the mean value is equal to zero. Larson et. al [3] describe the resulting modified stiffness matrix, and solution and load vector:

$$
\begin{bmatrix} \mathbf{K} & \mathbf{C}^{\mathrm{T}} \\ \mathbf{C} & 0 \end{bmatrix}
\begin{bmatrix} \mathbf{u} \\ \lambda \end{bmatrix} =
\begin{bmatrix} \mathbf{F} \\ 0 \end{bmatrix}
\tag{11}
$$

where $\mathbf{C}$ is a row vector of ones and λ may be though of as a force acting to enforce the constraints, which should be relatively small when compared to the values in the force vector and can be omitted from the solution vector.

4. Finite Element Formulations of Cross-Section Properties

4.1. Cross-Sectional Area

The area A of the cross-section is given by [2]:

$$
A = \int_A dx\,dy = \sum_e A_e = \sum_e \int_\Omega J_e\,d\eta\,d\xi\,d\zeta \tag{12}
$$

As the Jacobian is constant over the element, the integration over the element domain in Equation 12 can be performed using one point integration:

$$
A = \sum_e \sum_{i=1}^{1} w_i J_i \tag{13}
$$

4.2. First Moments of Area

The first moments of area are defined by:

$$
\begin{aligned}
Q_x &= \int_A y\,dA = \sum_e \int_\Omega \mathbf{N}\mathbf{y}_e J_e\,d\eta\,d\xi\,d\zeta \\
Q_y &= \int_A x\,dA = \sum_e \int_\Omega \mathbf{N}\mathbf{x}_e J_e\,d\eta\,d\xi\,d\zeta
\end{aligned}
\tag{14}
$$

where $\mathbf{x}_e$ and $\mathbf{y}_e$ are column vectors containing the cartesian coordinates of the element nodes. Equation 14 can be evaluated using three point integration as the shape functions ($\mathbf{N}$) are quadratic:

$$
\begin{aligned}
Q_x &= \sum_e \sum_{i=1}^{3} w_i \mathbf{N}_i \mathbf{y}_e J_e \\
Q_y &= \sum_e \sum_{i=1}^{3} w_i \mathbf{N}_i \mathbf{x}_e J_e
\end{aligned}
\tag{15}
$$

4.3. Centroids

The coordinates of the centroid are found from:

$$
\begin{aligned}
x_c &= \frac{Q_y}{A} \\
y_c &= \frac{Q_x}{A}
\end{aligned}
\tag{16}
$$

[2] Recall that the Jacobian is constant for the superparametric six-noded triangular element

4.4. Second Moments of Area

The second moments of area are defined by:

$$
\begin{aligned}
I_{xx} &= \int_A y^2\, dA = \sum_e \int_\Omega (\mathbf{N}\mathbf{y}_e)^2 J_e\, d\eta\, d\xi\, d\zeta \\
I_{yy} &= \int_A x^2\, dA = \sum_e \int_\Omega (\mathbf{N}\mathbf{x}_e)^2 J_e\, d\eta\, d\xi\, d\zeta \\
I_{xy} &= \int_A xy\, dA = \sum_e \int_\Omega \mathbf{N}\mathbf{y}_e \mathbf{N}\mathbf{x}_e J_e\, d\eta\, d\xi\, d\zeta
\end{aligned}
\tag{17}
$$

Equation 17 can be evaluated using six point integration as the square of the shape functions are quartic:

$$
\begin{aligned}
I_{xx} &= \sum_e \sum_{i=1}^{6} w_i (\mathbf{N}_i \mathbf{y}_e)^2 J_e \\
I_{yy} &= \sum_e \sum_{i=1}^{6} w_i (\mathbf{N}_i \mathbf{x}_e)^2 J_e \\
I_{xy} &= \sum_e \sum_{i=1}^{6} w_i \mathbf{N}\mathbf{y}_e \mathbf{N}\mathbf{x}_e J_e
\end{aligned}
\tag{18}
$$

Equation 18 lists the second moments of area about the global coordinate system axis, which is chosen arbitrarily by the user. These properties can be found about the centroidal axis of the cross-section by using the parallel axis theorem:

$$
\begin{aligned}
I_{\bar{x}\bar{x}} &= I_{xx} - {y_c}^2 A = I_{xx} - \frac{{Q_x}^2}{A} \\
I_{\bar{y}\bar{y}} &= I_{yy} - {x_c}^2 A = I_{yy} - \frac{{Q_y}^2}{A} \\
I_{\bar{x}\bar{y}} &= I_{xy} - x_c y_c A = I_{xy} - \frac{Q_x Q_y}{A}
\end{aligned}
\tag{19}
$$

4.5. Radii of Gyration

The radii of gyration can be calculated from the second moments of area and the cross-sectional area as follows:

$$
\begin{aligned}
r_x &= \sqrt{\frac{I_{xx}}{A}} \\
r_y &= \sqrt{\frac{I_{yy}}{A}}
\end{aligned}
\tag{20}
$$

4.6. Elastic Section Modulii

The elastic section modulii can be calculated from the second moments of area and the extreme (min. and max.) coordinates of the cross-section in the x and y-directions:

$$
\begin{aligned}
Z_{xx}^{+} &= \frac{I_{\bar{x}\bar{x}}}{y_{max} - y_c} \\
Z_{xx}^{-} &= \frac{I_{\bar{x}\bar{x}}}{y_c - y_{min}} \\
Z_{yy}^{+} &= \frac{I_{\bar{y}\bar{y}}}{x_{max} - x_c} \\
Z_{yy}^{-} &= \frac{I_{\bar{y}\bar{y}}}{x_c - x_{min}}
\end{aligned}
\tag{21}
$$

4.7. Plastic Section Modulii

For a homogenous section, the plastic centroid can be determined by by finding the intersection of the two lines that evenly divide the cross-sectional area in both the x and y directions. A suitable procedure could not be found in literature and thus an algorithm involving the iterative incrementation of the plastic centroid was developed. The algorithm is described in Figure 5.

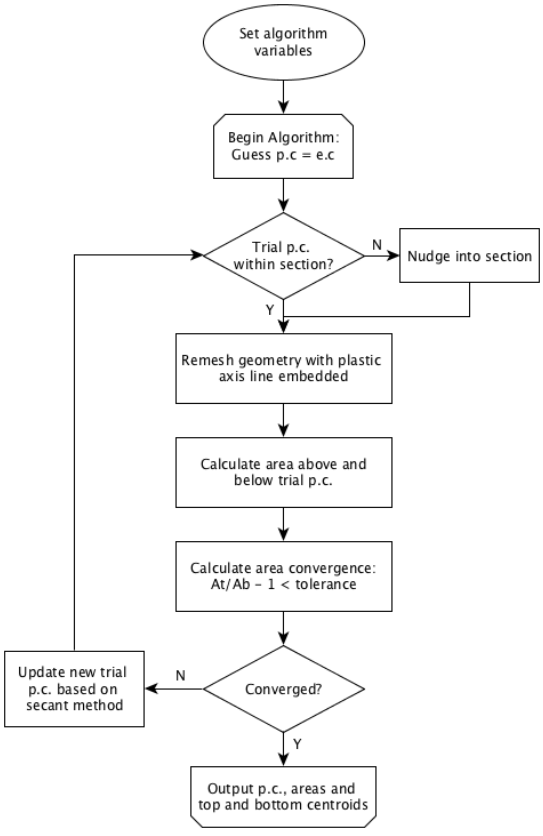

Figure 5: Algorithm used to calculate plastic neutral axis.

Once the plastic centroid has been located, the plastic section modulii can be readily computed using the following expression:

$$
\begin{aligned}
S_{xx} &= \frac{A}{2} \left| y_{c,t} - y_{c,b} \right| \\
S_{yy} &= \frac{A}{2} \left| x_{c,t} - x_{c,b} \right|
\end{aligned}
\tag{22}
$$

where A is the cross-sectional area, and $x_{c,t}$ and $x_{c,b}$ refer to the centroids of the top half section and bottom half section respectively.

4.8. Principal Axis Properties

The principal bending axes are determined by calculating the principal moments of inertia [2]:

$$\begin{aligned} I_{11} &= \frac{I_{\bar{x}\bar{x}} + I_{\bar{y}\bar{y}}}{2} + \Delta \\ I_{22} &= \frac{I_{\bar{x}\bar{x}} + I_{\bar{y}\bar{y}}}{2} - \Delta \end{aligned} \tag{23}$$

where:

$$\Delta = \sqrt{\left(\frac{I_{\bar{x}\bar{x}} - I_{\bar{y}\bar{y}}}{2}\right)^2 + {I_{\bar{x}\bar{y}}}^2} \tag{24}$$

The angle between the $\bar{x}$ axis and the axis belonging to the largest principal moment of inertia can be computed as follows:

$$\phi = \tan^{-1} \frac{I_{\bar{x}\bar{x}} - I_{11}}{I_{\bar{x}\bar{y}}} \tag{25}$$

The prinicpal section modulii require the calculation of the perpendicular distance from the principal axes to the extreme fibres. All the nodes in the mesh are considered with vector algebra used to compute the perpendicular distances and the minimum and maximum distances identified. The perpendicular distance from a point P to a line parallel to $\overrightarrow{u}$ that passes through Q is given by:

$$d = |\overrightarrow{PQ} \times \overrightarrow{u}| \tag{26}$$

The location of the point is checked to see whether it is above or below the principal axis. Again vector algebra is used to check this condition. The condition in Equation 27 will result in the point being above the $\overrightarrow{u}$ axis.

$$\overrightarrow{QP} \times \overrightarrow{u} < 0 \tag{27}$$

Using Equations 26 and 27, the principal section modulii can be calculated similar to Equations 21 and 22.

4.9. Torsion Constant

The Saint-Venant torsion constant (J_t) can be obtained by solving the partial differential equation in Equation 28 for the warping function, ω, subject to the boundary condition described in Equation 29.

$$\nabla^2 \omega = 0 \tag{28}$$

$$\frac{\partial \omega}{\partial x} n_x + \frac{\partial \omega}{\partial y} n_y = y n_x - x n_y \tag{29}$$

Pilkey [2] shows that by using the finite element method, this problem can be reduced to a set of linear equations of the form:

$$\mathbf{K}\boldsymbol{\omega} = \mathbf{F} \tag{30}$$

where $\mathbf{K}$ and $\mathbf{F}$ are assembled through summation at element level. The element equations for the eth element are:

$$\mathbf{k}^e \boldsymbol{\omega}^e = \mathbf{f}^e \tag{31}$$

with the stiffness matrix defined as:

$$\mathbf{k}^e = \int_\Omega \mathbf{B}^{\mathrm{T}} \mathbf{B} J_e \, d\eta \, d\xi \, d\zeta \tag{32}$$

and the load vector defined as:

$$\mathbf{f}^e = \int_\Omega \mathbf{B}^{\mathrm{T}} \begin{bmatrix} \mathbf{N}\mathbf{y} \\ -\mathbf{N}\mathbf{x} \end{bmatrix} J_e \, d\eta \, d\xi \, d\zeta \tag{33}$$

Applying numerical integration to Equations 32 and 33 results in the following expressions:

$$\begin{aligned} \mathbf{k}^e &= \sum_{i=1}^{3} w_i \mathbf{B}_i^{\mathrm{T}} \mathbf{B}_i J_e \\ \mathbf{f}^e &= \sum_{i=1}^{6} w_i \mathbf{B}_i^{\mathrm{T}} \begin{bmatrix} \mathbf{N}_i \mathbf{y}_e \\ -\mathbf{N}_i \mathbf{x}_e \end{bmatrix} J_e \end{aligned} \tag{34}$$

Once the warping function has been evaluated, the Saint-Venant torsion constant can be calculated as follows:

$$J = I_{xx} + I_{yy} - \boldsymbol{\omega}^{\mathrm{T}} \mathbf{K} \boldsymbol{\omega} \tag{35}$$

4.10. Shear Properties

The shear beahviour of the cross-section can be described by Saint-Venant's elasticity solution for a homogenous prismatic beam subjected to transverse shear loads [2]. Through cross-section equilibrium and linear-elasticity, an expression for the shear stresses resulting from a transverse shear load can be derived. Pilkey [2] explains that this is best done through the introduction of shear functions, Ψ and Φ, which describe the distribution of shear stress within a cross-section resulting from an applied transverse load in the x and y directions respectively. These shear functions can be obtained by solving the following uncoupled partial differential equations:

$$\begin{aligned} \nabla^2 \Psi &= 2(I_{\bar{x}\bar{y}} y - I_{\bar{x}\bar{x}} x) \\ \nabla^2 \Phi &= 2(I_{\bar{x}\bar{y}} x - I_{\bar{y}\bar{y}} y) \end{aligned} \tag{36}$$

subject to the respective boundary conditions:

$$\begin{aligned} \frac{\partial \Psi}{\partial n} &= \mathbf{n} \cdot \mathbf{d} \\ \frac{\partial \Phi}{\partial n} &= \mathbf{n} \cdot \mathbf{h} \end{aligned} \tag{37}$$

where $\mathbf{n}$ is the normal unit vector at the boundary and $\mathbf{d}$ and $\mathbf{h}$ are defined as follows:

$$\begin{aligned}\mathbf{d} &= \nu\left(I_{\bar{x}\bar{x}}\frac{x^2-y^2}{2} - I_{\bar{x}\bar{y}}xy\right)\mathbf{i} + \nu\left(I_{\bar{x}\bar{x}}xy + I_{\bar{x}\bar{y}}\frac{x^2-y^2}{2}\right)\mathbf{j} \\ \mathbf{h} &= \nu\left(I_{\bar{y}\bar{y}}xy - I_{\bar{x}\bar{y}}\frac{x^2-y^2}{2}\right)\mathbf{i} - \nu\left(I_{\bar{x}\bar{y}}xy + I_{\bar{y}\bar{y}}\frac{x^2-y^2}{2}\right)\mathbf{j}\end{aligned} \tag{38}$$

Pilkey [2] shows that the solution to Equation 36 subject to the boundary conditions in Equation 37 can be solved using the finite element method, resulting in a set of linear equations, at element level, of the form:

$$\begin{aligned}\mathbf{k}^e\boldsymbol{\Psi}^e &= \mathbf{f}_x^e \\ \mathbf{k}^e\boldsymbol{\Phi}^e &= \mathbf{f}_y^e\end{aligned} \tag{39}$$

The local stiffness matrix, $\mathbf{k}^e$, is identical to the matrix used to determine the torsion constant:

$$\mathbf{k}^e = \int_\Omega \mathbf{B}^{\mathrm{T}}\mathbf{B}J_e\, d\eta\, d\xi\, d\zeta \tag{40}$$

The load vectors are defined as:

$$\begin{aligned}\mathbf{f}_x^e &= \int_\Omega \left[\frac{\nu}{2}\mathbf{B}^{\mathrm{T}}\begin{bmatrix}d_1\\ d_2\end{bmatrix} + 2(1+\nu)\mathbf{N}^{\mathrm{T}}(I_{\bar{x}\bar{x}}\mathbf{N}\mathbf{x} - I_{\bar{x}\bar{y}}\mathbf{N}\mathbf{y})\right] J_e\, d\eta\, d\xi\, d\zeta \\ \mathbf{f}_y^e &= \int_\Omega \left[\frac{\nu}{2}\mathbf{B}^{\mathrm{T}}\begin{bmatrix}h_1\\ h_2\end{bmatrix} + 2(1+\nu)\mathbf{N}^{\mathrm{T}}(I_{\bar{y}\bar{y}}\mathbf{N}\mathbf{y} - I_{\bar{x}\bar{y}}\mathbf{N}\mathbf{x})\right] J_e\, d\eta\, d\xi\, d\zeta\end{aligned} \tag{41}$$

where:

$$\begin{aligned} d_1 &= I_{\bar{x}\bar{x}}r - I_{\bar{x}\bar{y}}q & d_2 &= I_{\bar{x}\bar{y}}r + I_{\bar{x}\bar{x}}q \\ h_1 &= -I_{\bar{x}\bar{y}}r + I_{\bar{y}\bar{y}}q & h_2 &= -I_{\bar{y}\bar{y}}r - I_{\bar{x}\bar{y}}q \\ r &= (\mathbf{N}\mathbf{x})^2 - (\mathbf{N}\mathbf{y})^2 & q &= 2\mathbf{N}\mathbf{x}\mathbf{N}\mathbf{y}\end{aligned}$$

Applying numerical integration to Equations 40 and 41 results in the following expressions:

$$\begin{aligned}\mathbf{k}^e &= \sum_{i=1}^{3} w_i\mathbf{B}_i^{\mathrm{T}}\mathbf{B}_i J_e \\ \mathbf{f}_x^e &= \sum_{i=1}^{6} w_i\left[\frac{\nu}{2}\mathbf{B}_i^{\mathrm{T}}\begin{bmatrix}d_{1,i}\\ d_{2,i}\end{bmatrix} + 2(1+\nu)\mathbf{N}_i^{\mathrm{T}}(I_{\bar{x}\bar{x}}\mathbf{N}_i\mathbf{x}_e - I_{\bar{x}\bar{y}}\mathbf{N}_i\mathbf{y}_e)\right] J_e \\ \mathbf{f}_y^e &= \sum_{i=1}^{6} w_i\left[\frac{\nu}{2}\mathbf{B}_i^{\mathrm{T}}\begin{bmatrix}h_{1,i}\\ h_{2,i}\end{bmatrix} + 2(1+\nu)\mathbf{N}_i^{\mathrm{T}}(I_{\bar{y}\bar{y}}\mathbf{N}_i\mathbf{y}_e - I_{\bar{x}\bar{y}}\mathbf{N}_i\mathbf{x}_e)\right] J_e\end{aligned} \tag{42}$$

4.10.1. Shear Centre

The shear centre can be computed consistently based on elasticity, or through Trefftz's definition, which is based on thin-wall assumptions [2].

Elasticity. Pilkey [2] demonstrates that the coordinates of the shear centre are given by the following expressions:

$$\begin{aligned}x_s &= \frac{1}{\Delta_s}\left[\frac{\nu}{2}\int_\Omega (I_{\bar{y}\bar{y}}x + I_{\bar{x}\bar{y}}y)\left(x^2+y^2\right)\, d\Omega - \int_\Omega \mathbf{g}\cdot\boldsymbol{\nabla}\boldsymbol{\Phi}\, d\Omega\right] \\ y_s &= \frac{1}{\Delta_s}\left[\frac{\nu}{2}\int_\Omega (I_{\bar{x}\bar{x}}y + I_{\bar{x}\bar{y}}x)\left(x^2+y^2\right)\, d\Omega + \int_\Omega \mathbf{g}\cdot\boldsymbol{\nabla}\boldsymbol{\Psi}\, d\Omega\right]\end{aligned} \tag{43}$$

where:

$$\begin{aligned}\Delta_s &= 2(1+\nu)(I_{\bar{x}\bar{x}}I_{\bar{y}\bar{y}} - {I_{\bar{x}\bar{y}}}^2) \\ \mathbf{g} &= y\mathbf{i} - x\mathbf{j}\end{aligned} \tag{44}$$

The first integral in Equation 43 can be evaluated using quadrature for each element. The second integral in Equation 43 can be simplified once the shear functions, Ψ and Φ, have been obtained:

$$\begin{aligned}\int_\Omega \mathbf{g}\cdot\boldsymbol{\nabla}\boldsymbol{\Phi}\, d\Omega &= \mathbf{F}^{\mathrm{T}}\boldsymbol{\Phi} \\ \int_\Omega \mathbf{g}\cdot\boldsymbol{\nabla}\boldsymbol{\Psi}\, d\Omega &= \mathbf{F}^{\mathrm{T}}\boldsymbol{\Psi}\end{aligned} \tag{45}$$

where $\mathbf{F}$ is the global load vector determined for the torsion problem in Equation 30. The resulting expression for the shear centre therefore becomes:

$$x_s = \frac{1}{\Delta_s}\left[\left(\frac{\nu}{2}\sum_{i=1}^{6} w_i(I_{\bar{y}\bar{y}}\mathbf{N}_i\mathbf{x}_e + I_{\bar{x}\bar{y}}\mathbf{N}_i\mathbf{y}_e)\Big((\mathbf{N}_i\mathbf{x}_e)^2 + (\mathbf{N}_i\mathbf{y}_e)^2\Big)J_e\right) - \mathbf{F}^{\mathrm{T}}\boldsymbol{\Phi}\right] \tag{46}$$

$$y_s = \frac{1}{\Delta_s}\left[\left(\frac{\nu}{2}\sum_{i=1}^{6} w_i(I_{\bar{x}\bar{x}}\mathbf{N}_i\mathbf{y}_e + I_{\bar{x}\bar{y}}\mathbf{N}_i\mathbf{x}_e)\Big((\mathbf{N}_i\mathbf{x}_e)^2 + (\mathbf{N}_i\mathbf{y}_e)^2\Big)J_e\right) + \mathbf{F}^{\mathrm{T}}\boldsymbol{\Psi}\right] \tag{47}$$

Trefftz's Definition. Using thin walled assumptions, the shear centre coordinates according to Trefftz's definition are given by:

$$\begin{aligned}x_s &= \frac{I_{\bar{x}\bar{y}}I_{x\omega} - I_{\bar{y}\bar{y}}I_{y\omega}}{I_{\bar{x}\bar{x}}I_{\bar{y}\bar{y}} - {I_{\bar{x}\bar{y}}}^2} \\ y_s &= \frac{I_{\bar{x}\bar{x}}I_{x\omega} - I_{\bar{x}\bar{y}}I_{y\omega}}{I_{\bar{x}\bar{x}}I_{\bar{y}\bar{y}} - {I_{\bar{x}\bar{y}}}^2}\end{aligned} \tag{48}$$

where the sectorial products of area are defined as:

$$\begin{aligned}I_{x\omega} &= \int_\Omega x\omega(x,y)\, d\Omega \\ I_{y\omega} &= \int_\Omega y\omega(x,y)\, d\Omega\end{aligned} \tag{49}$$

The finite element implementation of the integral in Equation 49 is shown below:

$$
\begin{aligned}
I_{x\omega} &= \sum_e \sum_{i=1}^{6} w_i \mathbf{N}_i \mathbf{x}_e \mathbf{N}_i \boldsymbol{\omega}_e J_e \\
I_{y\omega} &= \sum_e \sum_{i=1}^{6} w_i \mathbf{N}_i \mathbf{y}_e \mathbf{N}_i \boldsymbol{\omega}_e J_e
\end{aligned}
\tag{50}
$$

4.10.2. Shear Deformation Coefficients

The shear deformation coefficients are used to calculate the shear area of the section as a result of transverse loading. The shear area is defined as $A_s = k_s A$. Pilkey [2] describes the finite element formulation used to determine the shear deformation coefficients:

$$
\begin{aligned}
\kappa_x &= \sum_e \int_\Omega \left(\boldsymbol{\Psi}^{e\mathrm{T}} \mathbf{B}^{\mathrm{T}} - \mathbf{d}^{\mathrm{T}}\right)\left(\mathbf{B}\boldsymbol{\Psi}^e - \mathbf{d}\right) J_e \, d\Omega \\
\kappa_y &= \sum_e \int_\Omega \left(\boldsymbol{\Phi}^{e\mathrm{T}} \mathbf{B}^{\mathrm{T}} - \mathbf{h}^{\mathrm{T}}\right)\left(\mathbf{B}\boldsymbol{\Phi}^e - \mathbf{h}\right) J_e \, d\Omega \\
\kappa_{xy} &= \sum_e \int_\Omega \left(\boldsymbol{\Psi}^{e\mathrm{T}} \mathbf{B}^{\mathrm{T}} - \mathbf{d}^{\mathrm{T}}\right)\left(\mathbf{B}\boldsymbol{\Phi}^e - \mathbf{h}\right) J_e \, d\Omega
\end{aligned}
\tag{51}
$$

where the shear areas are related to κ_x and κ_y by:

$$
\begin{aligned}
k_{s,x}A &= \frac{{\Delta_s}^2}{\kappa_x} \\
k_{s,y}A &= \frac{{\Delta_s}^2}{\kappa_y} \\
k_{s,xy}A &= \frac{{\Delta_s}^2}{\kappa_{xy}}
\end{aligned}
\tag{52}
$$

The finite element formulation of Equation 51 is described in Equation 53.

$$
\begin{aligned}
\kappa_x &= \sum_e \sum_{i=1}^{6} w_i \left(\boldsymbol{\Psi}^{e\mathrm{T}} \mathbf{B}_i^{\mathrm{T}} - \frac{\nu}{2}\begin{bmatrix} d_{1,i} \\ d_{2,i} \end{bmatrix}^{\mathrm{T}}\right)\left(\mathbf{B}_i \boldsymbol{\Psi}^e - \frac{\nu}{2}\begin{bmatrix} d_{1,i} \\ d_{2,i} \end{bmatrix}\right) J_e \\
\kappa_y &= \sum_e \sum_{i=1}^{6} w_i \left(\boldsymbol{\Phi}^{e\mathrm{T}} \mathbf{B}_i^{\mathrm{T}} - \frac{\nu}{2}\begin{bmatrix} h_{1,i} \\ h_{2,i} \end{bmatrix}^{\mathrm{T}}\right)\left(\mathbf{B}_i \boldsymbol{\Phi}^e - \frac{\nu}{2}\begin{bmatrix} h_{1,i} \\ h_{2,i} \end{bmatrix}\right) J_e \\
\kappa_{xy} &= \sum_e \sum_{i=1}^{6} w_i \left(\boldsymbol{\Psi}^{e\mathrm{T}} \mathbf{B}_i^{\mathrm{T}} - \frac{\nu}{2}\begin{bmatrix} d_{1,i} \\ d_{2,i} \end{bmatrix}^{\mathrm{T}}\right)\left(\mathbf{B}_i \boldsymbol{\Phi}^e - \frac{\nu}{2}\begin{bmatrix} h_{1,i} \\ h_{2,i} \end{bmatrix}\right) J_e
\end{aligned}
\tag{53}
$$

4.10.3. Warping Constant

The warping constant, Γ, can be calculated from the warping function (ω) and the coordinates of the shear centre [2]:

$$
\Gamma = I_\omega - \frac{{Q_\omega}^2}{A} - y_s I_{x\omega} + x_s I_{y\omega} \tag{54}
$$

where the warping moments are calculated as follows:

$$
\begin{aligned}
Q_\omega &= \int_\Omega \omega \, d\Omega = \sum_e \sum_{i=1}^{3} w_i \mathbf{N}_i \boldsymbol{\omega}_e J_e \\
I_\omega &= \int_\Omega \omega^2 \, d\Omega = \sum_e \sum_{i=1}^{6} w_i (\mathbf{N}_i \boldsymbol{\omega}_e)^2 J_e
\end{aligned}
\tag{55}
$$

5. Cross-Section Stresses

Cross-section stresses resulting from an axial force, bending moments, a torsion moment and shear forces, can be evaluated at the integration points within each element. Section 3.4 describes the process of extrapolating the stresses to the element nodes and the combination of the results with the adjacent elements through nodal averaging.

5.1. Axial Stresses

The normal stress resulting from an axial force N_{zz} at any point i is given by:

$$
\sigma_{zz} = \frac{N_{zz}}{A} \tag{56}
$$

5.2. Bending Stresses

5.2.1. Global Axis Bending

The normal stress resulting from a bending moments M_{xx} and M_{yy} at any point i is given by [2]:

$$
\sigma_{zz} = -\frac{I_{\bar{x}\bar{y}} M_{xx} + I_{\bar{x}\bar{x}} M_{yy}}{I_{\bar{x}\bar{x}} I_{\bar{y}\bar{y}} - {I_{\bar{x}\bar{y}}}^2} \bar{x}_i + \frac{I_{\bar{y}\bar{y}} M_{xx} + I_{\bar{x}\bar{y}} M_{yy}}{I_{\bar{x}\bar{x}} I_{\bar{y}\bar{y}} - {I_{\bar{x}\bar{y}}}^2} \bar{y}_i \tag{57}
$$

5.2.2. Principal Axis Bending

Similarly, the normal stress resulting from a bending moments M_{11} and M_{22} at any point i is given by:

$$
\sigma_{zz} = -\frac{M_{22}}{I_{\bar{2}\bar{2}}} \bar{x}_{1,i} + \frac{M_{11}}{I_{\bar{1}\bar{1}}} \bar{y}_{2,i} \tag{58}
$$

5.3. Torsion Stresses

The shear stresses resulting from a torsion moment M_{zz} at any point i within an element e are given by [2]:

$$
\boldsymbol{\tau}^e = \begin{bmatrix} \tau_{zx} \\ \tau_{zy} \end{bmatrix}^e = \frac{M_{zz}}{J}\left(\mathbf{B}_i \boldsymbol{\omega}^e - \begin{bmatrix} \mathbf{N}_i \mathbf{y}_e \\ -\mathbf{N}_i \mathbf{x}_e \end{bmatrix}\right) \tag{59}
$$

5.4. Shear Stresses

The shear stresses resulting from transverse shear forces V_{xx} and V_{yy} at any point i within an element e are given by [2]:

$$
\begin{bmatrix} \tau_{zx} \\ \tau_{zy} \end{bmatrix}^e = \frac{V_{xx}}{\Delta_s}\left(\mathbf{B}_i \boldsymbol{\Psi}^e - \frac{\nu}{2}\begin{bmatrix} d_{1,i} \\ d_{2,i} \end{bmatrix}\right) + \frac{V_{yy}}{\Delta_s}\left(\mathbf{B}_i \boldsymbol{\Phi}^e - \frac{\nu}{2}\begin{bmatrix} h_{1,i} \\ h_{2,i} \end{bmatrix}\right) \tag{60}
$$

5.5. von Mises Stress

The von Mises stress can be determined from the net axial and shear stress as follows [2]:

$$\sigma_{vM} = \sqrt{{\sigma_{zz}}^2 + 3({\tau_{zx}}^2 + {\tau_{zy}}^2)} \tag{61}$$

6. Validation

The results from the python program were further validated through comparison with results obtained from the Strand7 beam section generator for the analysis of a doubly symmetric I-section and an asymmetric box section. The warping independent properties (Sections 4.8 to 4.1) showed exact agreement with the Strand7 results. The results for the warping dependent properties are summarised below, in which $\nu = 0$.

6.1. Doubly Symmetric I-Section

A straight edged doubly symmetric I-section was analysed for cross-sectional properties, with a depth of 200 mm, width of 100 mm, flange thickness of 10 mm and web thickness of 5 mm. A mesh was generated with a maximum area of 1 mm^2 as shown in Figure 6. The warping dependent properties are shown in Table 2 and are compared with the Strand7 results.

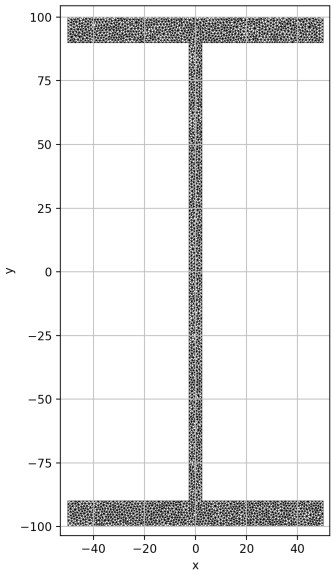

Figure 6: Mesh used for the determination of warping dependent properties for a doubly symmetric I-section.

Section Property	Python	Strand7	Variation
J [mm^4]	71217.28	71149.00	0.096%
I_w [mm^6]	1.5035×10^{10}	1.5035×10^{10}	0.003%
$A_{s,x}$ [mm^2]	1683.27	1683.67	0.024%
$A_{s,y}$ [mm^2]	942.54	942.61	0.007%

Table 2: Comparison of python and Strand7 results.

6.2. Asymmetric Box Section

A multi-core box section, no axes of symmetry, was analysed for cross-section properties, with a total width of 1300 mm, a depth of 300 mm and thickness of 50 mm. A mesh was generated with a maximum area of 50 mm^2 as shown in Figure 7. The warping dependent properties are shown in Table 3 and are compared with the Strand7 results. Figure 8 shows the various centroids from the python analysis.

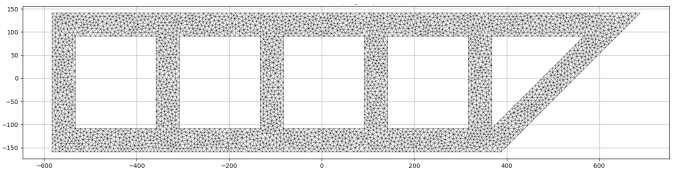

Figure 7: Mesh used for the determination of warping dependent properties for an asymmetric box section.

Section Property	Python	Strand7	Variation
J [mm^4]	5.7746×10^9	5.7685×10^9	0.106%
I_w [mm^6]	1.1726×10^{14}	1.1726×10^{14}	0.002%
$A_{s,11}$ [mm^2]	69923.98	69989.90	0.094%
$A_{s,22}$ [mm^2]	104830.80	104876.00	0.043%
$x_{s,11}$ [mm]	-21.6081	-21.6098	0.008%
$y_{s,22}$ [mm]	30.1824	30.1840	0.005%

Table 3: Comparison of python and Strand7 results.

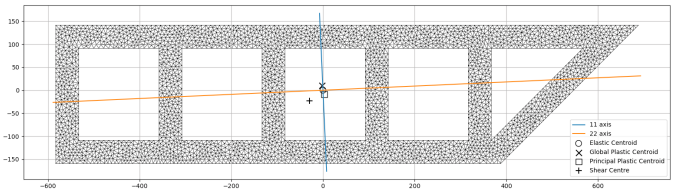

Figure 8: Elastic and plastic centroids, and shear centre for the asymmetric box section.

References

[1] C. A. Felippa, Introduction to Finite Element Methods, Department of Aerospace Engineering Sciences and Center for Aerospace Structures University of Colorado, Boulder, Colorado, 2004.

[2] W. D. Pilkey, Analysis and Design of Elastic Beams: Computational Methods, John Wiley & Sons, Inc., New York, 2002.

[3] M. G. Larson, F. Bengzon, The Finite Element Method: Theory, Implementation, and Applications, Vol. 10, Springer, Berlin, Heidelberg, 2013. doi:10.1007/978-3-642-33287-6.
URL `http://link.springer.com/10.1007/978-3-642-33287-6`